

Degenerate Higgs bosons: hiding a second Higgs at 125 GeV

Ning Chen¹ and Zuowei Liu^{2,3}

*¹Department of Modern Physics, University of Science
and Technology of China, Hefei, Anhui, 230026, China*

²School of Physics, Nanjing University, Nanjing, 210093, China

³Center for High Energy Physics, Tsinghua University, Beijing, 100084, China

chenning@ustc.edu.cn, zuoweiliu@nju.edu.cn

Abstract

More than one Higgs boson may be present near the currently discovered Higgs mass, which can not be properly resolved due to the limitations in the intrinsic energy resolution at the Large Hadron Collider. We investigated the scenarios where two CP -even Higgs bosons are degenerate in mass. To correctly predict the Higgs signatures, quantum interference effects between the two Higgs bosons must be taken into account, which, however, has been often neglected in the literature. We carried out a global analysis including the interference effects for a variety of Higgs searching channels at the Large Hadron Collider, which suggests that the existence of two degenerate Higgs bosons near 125 GeV is highly likely. Prospects of distinguishing the degenerate Higgs case from the single Higgs case are discussed.

PACS numbers:

I. INTRODUCTION

The discovery of the Higgs boson [1–3] with mass close to 125 GeV at the Larger Hadron Collider (LHC) [4, 5] completes the particle spectrum of the standard model (SM) [6]. The Higgs boson in the SM has been extremely successful in explaining the LHC data in various Higgs boson search channels [7]. Nonetheless, a richer structure beyond the simplest framework assumed in the SM may be present near 125 GeV, since one can not resolve the details of the spectrum near the Higgs boson mass with the current detection technology. The Higgs boson in the SM has a tiny decay width, about 4 MeV for mass near 125 GeV, which can not be directly measured via a scan on the lineshape of the Higgs boson resonance due to the limited energy resolution of the LHC. The Higgs boson decay modes with best energy resolution for mass reconstruction at the LHC are the ones with $\gamma\gamma$ and $ZZ \rightarrow \ell^+\ell^-\ell'^+\ell'^-$ as final states [8]. The energy resolution in photon, electron, and muon is of the order of $\sim\text{GeV}$ at the LHC [9–13], which is much larger than the total decay width of the SM Higgs boson. Moreover, the details of the Higgs sector remain largely unknown; a number of well-motivated theoretical models predict a Higgs sector that contains more than one scalar field.

In this work, we investigate the possibility that two CP -even Higgs bosons have nearly degenerate masses near 125 GeV. Both Higgs bosons contribute to the observed signal events in all Higgs searching channels that have been collected by the ATLAS and CMS collaborations in their $\sqrt{s} = 7$ TeV, $\sqrt{s} = 8$ TeV and $\sqrt{s} = 13$ TeV runs. Besides the individual contribution arising from the two Higgs bosons, the quantum interference effects of the two degenerate Higgs scalars must also be taken into consideration in order to correctly predict the signals at the LHC. To investigate the LHC signals, we take the two-Higgs-doublet model (2HDM) in which the degenerate Higgs scenarios can naturally arise as the prototype example, although our analysis can be extended to other models effortlessly.

The degenerate (or quasidegenerate) Higgs boson scenarios have been previously explored in the literature (see e.g. Refs. [14–16]). However, to our knowledge, the importance of the interference effects between the degenerate Higgs bosons have not been investigated before. In this work, we found that the quantum interference effects between the degenerate Higgs bosons can be rather substantial and can change the LHC signal predictions significantly. We further carried out a general global analysis in light of a variety of Higgs signal channels in the LHC runs with $\sqrt{s} = 7$

TeV and $\sqrt{s} = 8$ TeV,¹ and found that the existence of two degenerate Higgs bosons near 125 GeV is highly likely.

II. TWO HIGGS MEDIATORS IN DI-PHOTON SIGNAL

To illustrate the effects of the additional Higgs boson, we consider the dominant channel of observing the Higgs boson at the LHC, the gluon fusion process (denoted as ggF) with two photons in the final states. In the scenario where two CP -even Higgs bosons are degenerate in mass, both Higgs bosons enter as the s -channel mediators in the ggF process as shown in Fig. (1).

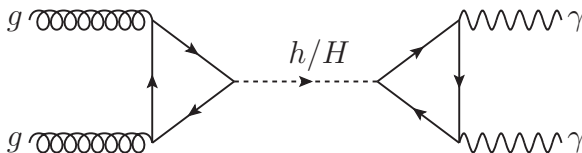


FIG. 1: Diphoton signal in the gluon fusion process.

We use h to denote the lighter Higgs boson and H the heavier one, with a small mass difference $\Delta M = M_H - M_h \geq 0$. To correctly calculate the cross section, we have to take into account both the Breit-Wigner formula and the interference terms of the Higgs propagators. In the ggF process, $gg \rightarrow h/H \rightarrow \gamma\gamma$, the parton-level cross section is given by

$$\hat{\sigma}(gg \rightarrow h/H \rightarrow \gamma\gamma) \propto \left| \sum_{\phi=h,H} \frac{G_{\phi gg} G_{\phi \gamma\gamma}}{\hat{s} - M_{\phi}^2 + iM_{\phi}\Gamma_{\phi}} \right|^2, \quad (1)$$

where $G_{\phi gg}$ and $G_{\phi \gamma\gamma}$ are the effective reduced couplings (dimensionless quantities with certain normalizations) of the Higgs boson ϕ to gluon and photon respectively, and M_{ϕ} (Γ_{ϕ}) is the mass (total decay width) of the Higgs boson ϕ . For the same process in the SM, only one Higgs boson contributes.

The total cross section at the LHC can be obtained via $\sigma_{\text{LHC}}(s) = \int d\tau \hat{\sigma}(\hat{s}) d\mathcal{L}/d\tau(\tau)$, where $\tau = \hat{s}/s$, $d\mathcal{L}/d\tau(\tau)$ is the parton luminosity. Because the Higgs decay widths are usually much smaller than the Higgs masses, i.e., $\Gamma_{\phi} \ll M_{\phi}$, only the integration in the vicinity of the Higgs mass is significant. The small variation in the parton luminosity near the Higgs mass can be safely

¹ The current $\sqrt{s} = 13$ TeV runs have only a few fb^{-1} data analyzed, which are less powerful in probing the Higgs boson(s) at the ~ 125 GeV scale than the 7 TeV and 8 TeV data, which have more than 20 fb^{-1} integrated luminosity combined, since the ratios in cross sections between 13 TeV and 8 TeV LHC runs are generally in the range (2 – 3).

neglected and the parton distribution functions can be well approximated by a fixed value at the Higgs mass in this case. Thus, the LHC cross section can be simplified as follows

$$\sigma_{\text{LHC}}(s) \propto \int d\hat{s} \hat{\sigma}(\hat{s}) \propto \sum_{A,B=h,H} \frac{G_{Agg} G_{A\gamma\gamma} G_{Bgg}^* G_{B\gamma\gamma}^*}{z_A - z_B^*}, \quad (2)$$

where $z_\phi \equiv M_\phi^2 - iM_\phi\Gamma_\phi$. To quantify the deviation from what expected in the SM, we normalize the LHC cross section by its corresponding SM value as follows

$$\mu = \sum_{A,B=h,H} \frac{G_{Agg} G_{A\gamma\gamma} G_{Bgg}^* G_{B\gamma\gamma}^*}{|G_{h^0gg} G_{h^0\gamma\gamma}|^2} \frac{z_{h^0} - z_{h^0}^*}{z_A - z_B^*}, \quad (3)$$

where h^0 is the SM Higgs boson. The μ value here contains four terms: the h contribution, the H contribution, and the h/H interference terms. Neglecting the interference terms, Eq. (3) is reduced to a sum of two terms

$$\mu = \frac{|\kappa_{hgg}\kappa_{h\gamma\gamma}|^2}{\Gamma_h/\Gamma_{h^0}} + \frac{|\kappa_{Hgg}\kappa_{H\gamma\gamma}|^2}{\Gamma_H/\Gamma_{h^0}}, \quad (4)$$

where we defined $\kappa_{\phi X} \equiv G_{\phi X}/G_{h^0 X}$ for any X state, and we have neglected the small mass difference between the Higgs bosons. The κ method given in Eq. (4) is often used in the literature to interpret experimental results for multiple Higgs boson scenarios. However, since the κ method ignores the important interference terms, it should be used with caution.

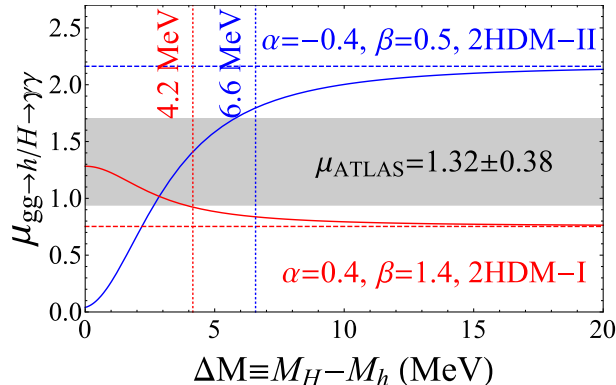


FIG. 2: (color online) Solid (dashed) curves are computed including (excluding) the interference terms. The gray band indicates the preferred μ range from ATLAS. Vertical dotted lines indicate the sum of the two Higgs decay widths, Γ .

To elucidate the effects due to interference and also the limitation of the κ method, signal strengths computed using both Eq. (3) and Eq. (4) for two model points are shown in Fig. (2). For both models, the naive κ method predicts a μ value disfavored by the ATLAS data, as shown

by the two horizontal dashed lines in Fig. (2). However, by including the interference effects, both models can actually give rise to a μ value within the ATLAS band for ΔM in the several MeV range. Fig. (2) shows that the interference effects are important for $\Delta M \lesssim \Gamma \equiv \Gamma_h + \Gamma_H$ (we will use Γ to denote the sum of the two Higgs decay widths throughout the paper) and can be either constructive as in the type-I 2HDM (hereafter 2HDM-I) model with $\alpha = 0.4$ and $\beta = 1.4$ or destructive as in the type-II 2HDM (hereafter 2HDM-II) model with $\alpha = -0.4$ and $\beta = 0.5$.

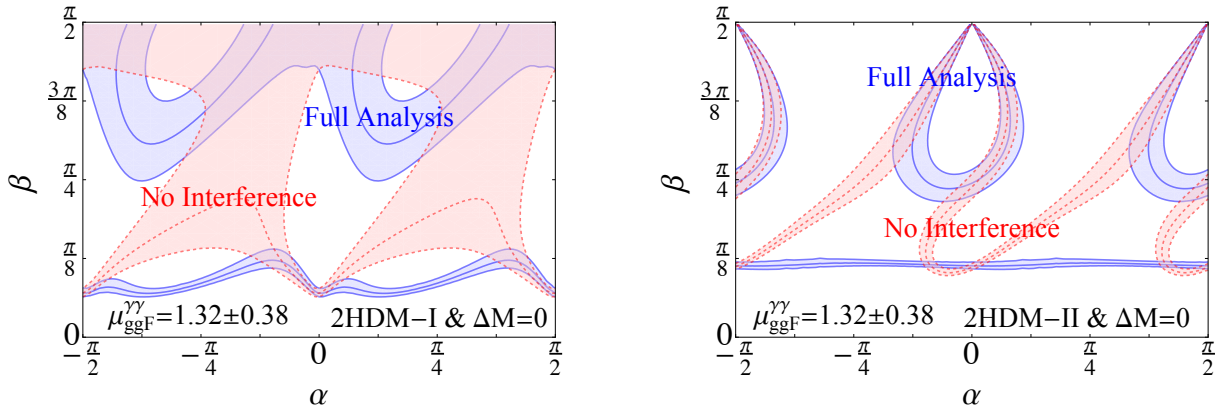


FIG. 3: (color online) Contours in the 2HDM-I (left) and the 2HDM-II (right) for the ATLAS measurement $\mu_{\text{ggF}}^{\gamma\gamma} = 1.32 \pm 0.38$, in the $\Delta M = 0$ case. The blue region enclosed by blue solid boundaries are the full calculation including the interference terms between the two Higgs bosons; the red region enclosed by red dashed boundaries are computed without the interference terms.

In Fig. (3), the contours computed via Eq. (3) and Eq. (4) are drawn to fit the signal strength for diphotons via the gluon fusion processes measured by the ATLAS detector. The two methods only overlap for a small fraction of the parameter space, as shown in Fig. (3). Clearly, the κ method can result in the parameter space where the signal strength has already been excluded by the ATLAS data, for example, the region near $\alpha = \pm \frac{\pi}{4}$ and $\beta = \frac{\pi}{4}$ in the 2HDM-I as shown in the left panel of Fig. (3). Thus, analysis with the κ method is inadequate in dealing with two degenerate Higgs bosons, since it can lead to erroneous conclusions.

III. GLOBAL ANALYSIS

To analyze the limits from LHC data, we carry out a global χ^2 analysis for a variety of Higgs searching channels. We categorize the experimental data in terms of the Higgs production channels (hereafter P) and Higgs decay final states (hereafter D). There are six major production channels: $P=(\text{ggF}, \text{VBF}, \text{WH}, \text{ZH}, \text{ttH}, \text{bbH})$, where VBF stands for the vector boson fusion processes,

D	P	$\mu \pm \sigma$			
		ATLAS	Ref	CMS	Ref
$\gamma\gamma$	ggF	1.32 ± 0.38	[17]	$1.12^{+0.37}_{-0.32}$	[23]
$\gamma\gamma$	VBF	0.8 ± 0.7	[17]	$1.58^{+0.77}_{-0.68}$	[23]
$\gamma\gamma$	WH	1.0 ± 1.6	[17]	-	-
$\gamma\gamma$	ZH	$0.1^{+3.7}_{-0.1}$	[17]	-	-
$\gamma\gamma$	VH	-	-	$-0.16^{+1.16}_{-0.79}$	[23]
$\gamma\gamma$	ttH	$1.6^{+2.7}_{-1.8}$	[17]	$2.69^{+2.51}_{-1.81}$	[23]
ZZ	ggF,ttH,bbH	$1.7^{+0.5}_{-0.4}$	[18]	-	-
ZZ	ggF,ttH	-	-	$0.80^{+0.46}_{-0.36}$	[24]
ZZ	VBF,VH	$0.3^{+1.6}_{-0.9}$	[18]	$1.7^{+2.2}_{-2.1}$	[24]
WW	ggF	$1.02^{+0.29}_{-0.26}$	[19]	$0.74^{+0.22}_{-0.20}$	[25]
WW	VBF	$1.27^{+0.53}_{-0.45}$	[19]	$0.60^{+0.57}_{-0.46}$	[25]
WW	VH	-	-	$0.39^{+1.97}_{-1.87}$	[25]
bb	ttH	1.5 ± 1.1	[20]	$1.2^{+1.6}_{-1.5}$	[26]
bb	VH	$0.51^{+0.40}_{-0.37}$	[21]	1.0 ± 0.5	[27]
$\tau\tau$	ggF	$2.0^{+1.5}_{-1.2}$	[22]	1.07 ± 0.46	[28]
$\tau\tau$	VBF,VH	$1.24^{+0.59}_{-0.54}$	[22]	-	-
$\tau\tau$	VBF	-	-	0.94 ± 0.41	[28]
$\tau\tau$	VH	-	-	-0.33 ± 1.02	[28]

TABLE I: Signal strengths of Higgs searches measured by the ATLAS and CMS collaborations, for various decay and production channels for the $\sqrt{s}=7$ TeV and $\sqrt{s}=8$ TeV runs.

including both WBF and ZBF, and the last four processes are the ones in which Higgs is produced in association with other particle(s) as indicated. There are five major decay final states used to detect the Higgs boson, which are $D=(\gamma\gamma, ZZ, WW, bb, \tau\tau)$. The ZZ and WW final states are usually tagged with 4ℓ and $2\ell 2\nu$, respectively. A list of the major experimental results combining the 7 TeV data and the 8 TeV data in various Higgs searching channels from both ATLAS and CMS collaborations, are summarized in Table (I). The experimental results are expressed in term of the signal strength, which is the ratio between the observed LHC signal events and its SM expectation.

The signal strength in the 2HDM for given production and decay channel (denoted by μ_{PD})

can be computed via

$$\mu_{\text{PD}} = \sum_{A,B=h,H} \frac{G_{AL}G_{AD}G_{BL}^*G_{BD}^*}{|G_{h^0L}G_{h^0D}|^2} \frac{z_{h^0} - z_{h^0}^*}{z_A - z_B^*}, \quad (5)$$

where G_{AL} is the reduced coupling constant between the mediator A and the state L , and so on. For the production channels $P=(ggF, ttH, bbH)$, the corresponding L states are $L = (gg, tt, bb)$; for $P=(\text{VBF}, WH, ZH)$, we have $L = VV$ in the 2HDM [29]. For completeness, we prove the validation of using Eq. (5) for the WH and ZH processes in the Appendix.

The reduced Higgs couplings to up-type quarks and to W and Z bosons are the same for both 2HDM-I and 2HDM-II: $G_{h^0uu} = \cos \alpha / \sin \beta$ and $G_{H^0uu} = \sin \alpha / \sin \beta$; $G_{h^0VV} = \sin(\beta - \alpha)$ and $G_{H^0VV} = \cos(\beta - \alpha)$. For down-type quarks, $G_{h^0dd} = \cos \alpha / \sin \beta$ and $G_{H^0dd} = \sin \alpha / \sin \beta$ for 2HDM-I; $G_{h^0dd} = -\sin \alpha / \cos \beta$ and $G_{H^0dd} = \cos \alpha / \cos \beta$ for 2HDM-II. The charged leptons have the same reduced coupling constant as the down-type quarks. For a review on the 2HDM, see e.g. Refs. [30–32]. In the SM, we have $G_{h^0X} = 1$ for all the above couplings.

For Higgs couplings to gluon and photon, loop contributions via fermions and vector bosons are calculated. The reduced couplings to gluons for both h and H in the 2HDM and for h^0 in the SM are given by $G_{\phi gg} = G_{\phi uu}A_{1/2}(x_{\phi t}) + G_{\phi dd}A_{1/2}(x_{\phi b})$ where $A_{1/2}(x)$ is the fermion loop function, $x_{\phi p} \equiv M_p^2/(4M_p^2)$ with M_p being the mass of the circulating particle. The reduced couplings to photons are given by $G_{\phi \gamma \gamma} = N_c Q_u^2 G_{\phi uu} A_{1/2}(x_{\phi t}) + N_c Q_d^2 G_{\phi dd} A_{1/2}(x_{\phi b}) + G_{\phi VV} A_1(x_{\phi W})$ where $N_c = 3$, $Q_u = 2/3$, $Q_d = -1/3$, and $A_1(x)$ is the vector boson loop function. The loop functions $A_{1/2}(x)$ and $A_1(x)$ can be found in e.g. Refs. [30, 31]. Here we include the bottom quark loops, because they can become significant in the 2HDM-II for large $\tan \beta$.

For the SM Higgs boson decay width, we use $\Gamma_{h^0} = 4.07$ MeV as the total width for $M_{h^0} = 125$ GeV [33]. The partial decay widths are obtained by multiplying the total width with the following branching ratios: $\text{BR}(bb, \tau\tau, \mu\mu, cc, ss) = (5.77 \times 10^{-1}, 6.32 \times 10^{-2}, 2.19 \times 10^{-4}, 2.91 \times 10^{-2}, 2.46 \times 10^{-4})$ for fermions, and $\text{BR}(gg, \gamma\gamma, Z\gamma, WW, ZZ) = (8.57 \times 10^{-2}, 2.28 \times 10^{-3}, 1.54 \times 10^{-3}, 2.15 \times 10^{-1}, 2.64 \times 10^{-2})$ for bosons [33]. The partial decay widths of h and H in the 2HDM are computed via $\Gamma(\phi \rightarrow X) = \Gamma(h^0 \rightarrow X) |G_{\phi X} / G_{h^0 X}|^2$ for any X final state.

For most ATLAS and CMS analyses given in Table (I), the μ value for one single production channel is provided. There are also signal strengths for multiple production channels. For such analyses involving several production channels, we compute the signal strength as follows

$$\mu_{\text{multiple}} = \sum_P \mu_{\text{PD}} N_{\text{PD}}^{\text{SM}} / \sum_P N_{\text{PD}}^{\text{SM}}, \quad (6)$$

where $N_{\text{PD}}^{\text{SM}} = \mathcal{L}_7 \sigma_{\text{PD}}^{\text{SM-7}} (A\epsilon)_{\text{PD}}^7 + \mathcal{L}_8 \sigma_{\text{PD}}^{\text{SM-8}} (A\epsilon)_{\text{PD}}^8$ is the expected number of events for the SM case

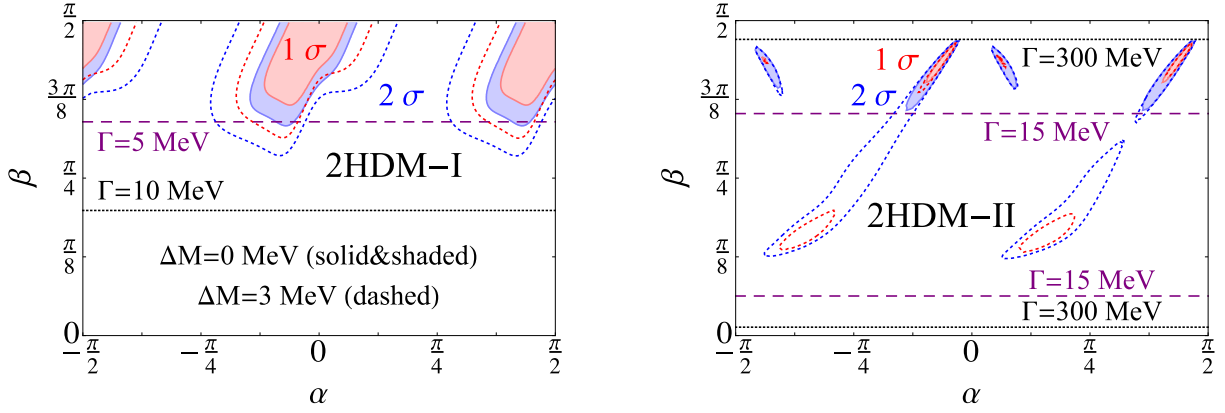


FIG. 4: (color online) Contours of χ^2_{LHC} in the 2HDM-I (left) and the 2HDM-II (right) for $\Delta M = 0$ (solid & shaded) and $\Delta M = 3$ MeV (dashed) cases. The horizontal lines indicate the sum of the decay widths Γ .

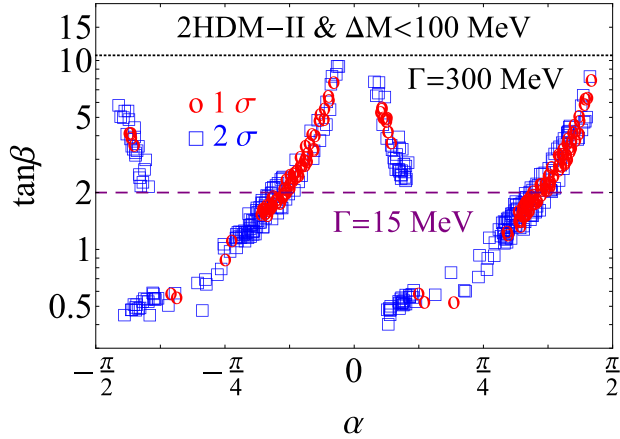


FIG. 5: (color online) Models within 1σ and 2σ corridors in χ^2 near the best-fit model for the $\Delta M < 100$ MeV case.

at the LHC. Here $\sigma_{\text{PD}}^{\text{SM-7}}$ and \mathcal{L}_7 are the SM production cross section and the integrated luminosity at the $\sqrt{s} = 7$ TeV LHC, and so on. In analyses combining the VBF and VH processes, we have $\mu_{\text{multiple}} = \mu_{\text{PD}}$, since the signal strengths are the same for these processes. Thus in Table (I), the processes in which we have to take into account the SM number of events $N_{\text{PD}}^{\text{SM}}$ are the ZZ final states with $\text{ggF}+\text{ttH}+\text{bbH}$ (ATLAS) and $\text{ggF}+\text{ttH}$ (CMS). The integrated luminosities are 4.5 and 20.3 fb^{-1} for $\sqrt{s}=7$ and 8 TeV respectively in the $\text{ggF}+\text{ttH}+\text{bbH}$ (ATLAS), and 5.1 and 19.7 fb^{-1} for $\text{ggF}+\text{ttH}$ (CMS).

For the SM production cross sections, we use $\sigma_{\text{SM}} = (15.13, 1.222, 0.5785, 0.3351, 0.08632, 0.1558)$ pb [34] for the (ggF, VBF, WH, ZH, ttH, bbH) processes respectively with LHC $\sqrt{s}=7$

TeV, and $\sigma_{\text{SM}} = (19.27, 1.578, 0.7046, 0.4153, 0.1293, 0.2035)$ pb [35] with LHC $\sqrt{s}=8$ TeV. The SM cross sections for specific final states are calculated via $\sigma_{\text{PD}}^{\text{SM}} = \sigma_P^{\text{SM}}\text{BR}(h^0 \rightarrow D)$.

For these analyses combining different production channels, we assume the detector acceptances and efficiencies to be the same for different production channels and for different center-of-mass energies at the LHC. Thus, when computing the signal strength μ_{multiple} for multiple processes, the detector acceptances and efficiencies ($A\epsilon$) cancel in the numerator and the denominator of Eq. (6) and do not affect the signal strength. To fully address the effects due to the detector acceptances and efficiencies for different processes and colliding energies requires a careful simulation, which is beyond the scope of this paper. We believe that neglecting the effects of the detector efficiency in the two analyses with ZZ final states does not alter the conclusion of our analysis significantly.

To quantitatively evaluate how well a model fits the LHC data, we compute χ^2 as follows

$$\chi^2 = \sum_i \left(\frac{\mu_{\text{th}}^i - \mu_{\text{data}}^i}{\sigma_{\text{data}}^i} \right)^2, \quad (7)$$

where μ_{th}^i is the predicted signal strength in theory models, and μ_{data}^i and σ_{data}^i are the signal strengths and the associated uncertainties for the decay and production channels given in Table (I).

Model	Type	α	β	ΔM	χ_{ATLAS}^2	χ_{CMS}^2	χ_{LHC}^2
	SM	-	-	-	7.2	6.8	14.0
A	I	-0.35	1.36	0	6.0	11.5	17.5
B	I	-0.13	1.30	0	7.7	6.4	14.1
C	I	-0.12	1.40	0	7.3	6.6	13.9
E	II	-1.45	1.44	0	4.3	15.7	20.0
F	II	-0.21	1.38	0	10.0	6.3	16.3
G	II	-0.166	1.40	0	6.5	7.3	13.8
M	I	-0.26	1.23	5	6.8	6.8	13.7
N	II	-1.11	0.49	2.7	6.6	6.5	13.0

TABLE II: Benchmark models. ΔM in unit of MeV.

The SM has $\chi^2 = 14$ with $\chi^2 = 7.2$ (6.8) for ATLAS (CMS) measurements. In the 2HDM-I with $\Delta M = 0$, the best-fit models give $\chi_{\text{min}}^2 = 6.0, 6.4, 13.9$ for ATLAS, CMS, and both measurements. In the 2HDM-II with $\Delta M = 0$, the best-fit models give $\chi_{\text{min}}^2 = 4.3, 6.3, 13.8$ for ATLAS, CMS, and both measurements. Thus, the 2HDM-I and 2HDM-II can provide a fit to data somewhat better

than the SM. Several benchmark model points with vanishing and non-vanishing ΔM are provided in Table (II).

We carry out a full χ^2 analysis in the 2HDM parameter space spanned by α and β ,² with both ATLAS and CMS data given in Table (I). The 1σ and 2σ contours are plotted with $\Delta\chi^2 = 2.3$ and 6.18, for the $\Delta M = 0$ and $\Delta M = 3$ MeV cases, in Fig. (4). For the $\Delta M = 0$ case, in both 2HDM-I and 2HDM-II models, the preferred model points reside in the large $\tan\beta$ region. The sum of the decay widths Γ is less than 5 MeV for the preferred 2HDM-I models, whereas in the 2HDM-II, the preferred models have $15\text{ MeV} \lesssim \Gamma \lesssim 300\text{ MeV}$. When $\Delta M = 0$ is increased to 3 MeV, the preferred 2HDM-I parameter space expands around its previously preferred regions; however, under the same ΔM increase in 2HDM-II, new parameter regions appear. We note in passing that the current Higgs mass measurement at the LHC has an uncertainty of ~ 240 MeV [8], which, however, does not rule out the 2HDM-II models with $\Gamma > 240$ MeV, because the analysis is carried out with SM assumptions and is not model-independent. Nevertheless, further reducing the mass uncertainties at the LHC can probe the preferred region of the 2HDM-II parameter space.

The interference effects between the two Higgs bosons depend strongly on the ratio $\Delta M/\Gamma$; when the mass separation ΔM becomes significantly large compared with the sum of the decay widths Γ , the interference effects begin to diminish, as illustrated in Fig. (2). In the two types of 2HDM considered, the dependence of Γ on the angle α is negligible; the dependence of Γ on the β angle is significant and can be well approximated as follows: $\Gamma/\Gamma_{h^0} \simeq 1 + (1 - \text{BR}_{VV})/\tan^2\beta$ for the 2HDM-I, and $\Gamma/\Gamma_{h^0} \simeq 1 + (\text{BR}_{cc} + \text{BR}_{gg})/\tan^2\beta + \tan^2\beta(\text{BR}_{bb} + \text{BR}_{\tau\tau})$ for the 2HDM-II, where the BRs denote the Higgs boson decay branching ratios in the SM.

To explore models with non-vanishing ΔM , we carry out a three dimensional random scan with flat priors in $-\frac{\pi}{2} \leq \alpha \leq \frac{\pi}{2}$, $0 \leq \beta \leq \frac{\pi}{2}$, and $\Delta M < 100$ MeV. Fig. (5) shows the 2HDM-II models that fall in the 1σ and 2σ region from the scan. These models all have $\tan\beta < 10$, which corresponds roughly to $\Gamma \lesssim 300$ MeV, consistent with the upper value in Fig. (4). There are two major bands of model points within 1σ and 2σ corridors in the random scan: $\beta = \alpha + \frac{\pi}{2}$, and $\beta = \alpha$. The former case has $\cos(\beta - \alpha) = 0$ which is also known as the ‘‘alignment’’ limit, and the latter case has $\sin(\beta - \alpha) = 0$. In the former case, the coupling strength (normalized to SM values) between h and SM particles are $(1, 1, 1, 1)$ for (vector bosons, up-type quarks, down-type quarks, charged leptons), and the ones between H and SM particles are $(0, 1/\tan\beta, -\tan\beta, -\tan\beta)$ respectively.

² Plots with $\cos(\beta - \alpha)$ and β (or $\tan\beta$) as axes are sometimes used. However, one model point in the parameter space spanned by $\cos(\beta - \alpha)$ and β can correspond to two different model points in the parameter space spanned by α and β . Thus the interpretation on the variable $\cos(\beta - \alpha)$ is ambiguous and it should not be used.

In the latter case, the coupling strength between H and SM particles are $(1, 1, 1, 1)$, and the ones between h and SM particles are $(0, -1/\tan\beta, \tan\beta, \tan\beta)$, as in the order given before. These two bands are also exhibited in Fig. (4).

The best-fit model in the 2HDM-I prefers to go to much large ΔM values, such that our approximation no longer holds. Here we provide a 2HDM-I benchmark model with small mass difference in Table (II): model point M with $\Delta M = 5$ MeV. Unlike the 2HDM-I, the best-fit model in the 2HDM-II has $\Delta M \simeq 2.7$ MeV, which is represented by model point N in Table (II).

IV. HIGGS WIDTH AND LEPTON COLLIDER

The total decay width of the SM Higgs boson can be indirectly constrained by comparing the off-peak Higgs to ZZ events with the on-peak ones [36]. However, this method can not be used to constrain the decay widths of the degenerate Higgs bosons, because this indirect method is based on the SM assumptions. A direct measurement of the Higgs width can be achieved in a muon collider by scanning the lineshape of the Higgs resonance, where one can unambiguously determine whether more than one scalar is present. It is anticipated that a 4 % accuracy on the SM-like Higgs boson width can be achieved in a future muon collider with 0.003% beam energy resolution and 1 fb^{-1} integrated luminosity [37]. At future e^+e^- collider, the total Higgs width can be indirectly inferred via the $H \rightarrow WW$ process to a precision of (4-5)% [38]. A clean and model-independent method to determine the Higgs mass is to reconstruct the recoil mass in the Higgs-strahlung process $e^+e^- \rightarrow h^0 Z$, which can probe the SM Higgs mass at the International Linear Collider (ILC), at future FCC-ee, and at the Circular Electron Positron Collider (CEPC). A precision of $\delta M_{h^0} \simeq 5.9$ MeV in the SM is expected at the CEPC [39]. However, the measurements at the e^+e^- colliders discussed above are indirect and should be interpreted based on the underlying theory models; the precision discussed for the lepton collider are only applicable to a single SM Higgs boson case. Thus, the discrimination power regarding the degenerate Higgs bosons at electron collider is rather limited.

V. CONCLUSION

In this work, we have analyzed the LHC signals arising from the scenario where two CP -even Higgs bosons are almost degenerate in mass near 125 GeV. The quantum interference effects between degenerate Higgs bosons have to be taken into account in order to correctly predict

the LHC signal, which, however, was often neglected in the literature. We have taken 2HDM-I and 2HDM-II as prototype models for our concrete numerical analysis; for certain regions in the parameter space, the interference effects can alter the predictions significantly. We have carried out a global χ^2 analysis using 27 measurements on Higgs signal strengths by ATLAS and CMS collaborations, which shows that the 2HDM with two degenerate CP -even Higgs bosons can fit the LHC data somewhat better than the SM. Future LHC data can improve the Higgs measurements with better accuracy, but it lacks the capability of distinguishing the two Higgs bosons that are degenerate in mass. It is also quite challenging to fully resolve this issue in the proposed e^+e^- colliders. Nevertheless, for specific models, such as the 2HDM, analyses employing multiple collider searching channels with more LHC data (and/or data from future e^+e^- colliders) can further constrain the parameter space or even completely rule out the entire parameter space, but such results are model-dependent. To unambiguously discriminate the degenerate Higgs case from the single Higgs case, one may have to go to a future muon collider, where a scan around the Higgs resonance can be performed.

Acknowledgements

We thank Yan-Wen Liu, Ning Zhou for helpful discussions. N.C. is partially supported by National Science Foundation of China (under Grant No. 11335007, 11575176), and the Fundamental Research Funds for the Central Universities (under Grant No. WK2030040069). The work of Z.L. is supported in part by the Nanjing University Grant 22721007 and the Tsinghua University Grant 523081007.

VI. APPENDIX: THE INTEGRAL FOR $2 \rightarrow 3$ PHASE SPACE

The signal strength in Eq. (5) is generalized from the results for the ggF production channel to two photons in Eq. (3). Here, we prove that Eq. (5) is also valid for evaluating the signal strength for the WH and ZH processes. Specifically, we consider the process of $q\bar{q}' \rightarrow V^* \rightarrow (h/H \rightarrow f\bar{f})V$, whose parton-level amplitude reads

$$i\mathcal{M} \sim \bar{v}(p_1)\gamma^\mu(g_V + g_A\gamma_5)u(p_2)\frac{-i}{\hat{s} - m_V^2}\epsilon_\mu^*(k) \times \bar{u}(q_1) \sum_{A=h,H} \left(\frac{G_{AVV}}{q^2 - M_A^2 + iM_A\Gamma_A} G_{Aff} \right) v(q_2). \quad (8)$$

We find that the integral of the amplitude squared over the $2 \rightarrow 3$ phase space is reduced to the integral over the energy of the final-state vector boson E_k as follows

$$\int |\mathcal{M}|^2 d\text{PS}_{2 \rightarrow 3} \sim \frac{1}{4m_V^2(\hat{s} - m_V^2)^2} \int dE_k f(E_k) \sum_{A,B=h,H} \frac{G_{AVV} G_{Aff} G_{BVV}^* G_{Bff}^*}{E_k - E_k^{A*} E_k - E_k^B}, \quad (9)$$

where

$$f(E_k) = \sqrt{E_k^2 - m_V^2} \left[(\hat{s} - E_k \sqrt{\hat{s}})(2E_k^2 + m_V^2) + 12M_\phi^2 m_V^2 \right], \quad (10a)$$

$$E_k^\phi = \frac{1}{2\sqrt{\hat{s}}} (\hat{s} + m_V^2 - M_\phi^2 - iM_\phi \Gamma_\phi). \quad (10b)$$

Since the decay width is much smaller than the Higgs boson masses, $\Gamma_\phi \ll M_\phi$, only the E_k values leading to the on-shell Higgs boson (i.e., $q^2 = M_\phi^2$) contribute significantly to the integral. Thus, we can fix the E_k values in the function $f(E_k)$ and move it outside of the integral such that

$$\int |\mathcal{M}|^2 d\text{PS}_{2 \rightarrow 3} \sim \frac{1}{4m_V^2(\hat{s} - m_V^2)^2} f(E_k^0) \int dE_k \sum_{A,B=h,H} \frac{G_{AVV} G_{Aff} G_{BVV}^* G_{Bff}^*}{E_k - E_k^{A*} E_k - E_k^B} \quad (11)$$

The remaining integral can be computed via the residue theorem

$$\int \frac{dE_k}{(E_k - E_k^{A*})(E_k - E_k^B)} = \frac{2\pi i}{E_k^{A*} - E_k^B} = \frac{4\pi i \sqrt{\hat{s}}}{z_B^* - z_A}, \quad (12)$$

which has the same dependence on z_ϕ as Eq. (2). Thus, we can obtain exactly the same expression for μ as in Eq. (3) for the WH and ZH processes.

-
- [1] P. W. Higgs, Phys. Lett. **12**, 132 (1964).
 - [2] P. W. Higgs, Phys. Rev. Lett. **13**, 508 (1964).
 - [3] F. Englert and R. Brout, Phys. Rev. Lett. **13**, 321 (1964).
 - [4] G. Aad *et al.* [ATLAS Collaboration], Phys. Lett. B **716**, 1 (2012) doi:10.1016/j.physletb.2012.08.020 [arXiv:1207.7214 [hep-ex]].
 - [5] S. Chatrchyan *et al.* [CMS Collaboration], Phys. Lett. B **716**, 30 (2012) doi:10.1016/j.physletb.2012.08.021 [arXiv:1207.7235 [hep-ex]].
 - [6] S. Weinberg, Phys. Rev. Lett. **19**, 1264 (1967).
 - [7] The ATLAS and CMS Collaborations, ATLAS-CONF-2015-044.
 - [8] G. Aad *et al.* [ATLAS and CMS Collaborations], Phys. Rev. Lett. **114**, 191803 (2015) doi:10.1103/PhysRevLett.114.191803 [arXiv:1503.07589 [hep-ex]].
 - [9] G. Aad *et al.* [ATLAS Collaboration], Eur. Phys. J. C **74**, no. 10, 3071 (2014) doi:10.1140/epjc/s10052-014-3071-4 [arXiv:1407.5063 [hep-ex]].

- [10] G. Aad *et al.* [ATLAS Collaboration], *Eur. Phys. J. C* **74**, no. 11, 3130 (2014) doi:10.1140/epjc/s10052-014-3130-x [arXiv:1407.3935 [hep-ex]].
- [11] S. Chatrchyan *et al.* [CMS Collaboration], *JINST* **7**, P10002 (2012) doi:10.1088/1748-0221/7/10/P10002 [arXiv:1206.4071 [physics.ins-det]].
- [12] V. Khachatryan *et al.* [CMS Collaboration], *JINST* **10**, no. 06, P06005 (2015) doi:10.1088/1748-0221/10/06/P06005 [arXiv:1502.02701 [physics.ins-det]].
- [13] V. Khachatryan *et al.* [CMS Collaboration], *JINST* **10**, no. 08, P08010 (2015) doi:10.1088/1748-0221/10/08/P08010 [arXiv:1502.02702 [physics.ins-det]].
- [14] J. F. Gunion, Y. Jiang and S. Kraml, *Phys. Rev. D* **86**, 071702 (2012) doi:10.1103/PhysRevD.86.071702 [arXiv:1207.1545 [hep-ph]].
- [15] J. F. Gunion, Y. Jiang and S. Kraml, *Phys. Rev. Lett.* **110**, no. 5, 051801 (2013) doi:10.1103/PhysRevLett.110.051801 [arXiv:1208.1817 [hep-ph]].
- [16] N. Craig, J. Galloway and S. Thomas, arXiv:1305.2424 [hep-ph].
- [17] G. Aad *et al.* [ATLAS Collaboration], *Phys. Rev. D* **90**, no. 11, 112015 (2014) [arXiv:1408.7084 [hep-ex]].
- [18] G. Aad *et al.* [ATLAS Collaboration], *Phys. Rev. D* **91**, no. 1, 012006 (2015) [arXiv:1408.5191 [hep-ex]].
- [19] G. Aad *et al.* [ATLAS Collaboration], *Phys. Rev. D* **92**, no. 1, 012006 (2015) [arXiv:1412.2641 [hep-ex]].
- [20] G. Aad *et al.* [ATLAS Collaboration], *Eur. Phys. J. C* **75**, no. 7, 349 (2015) [arXiv:1503.05066 [hep-ex]].
- [21] G. Aad *et al.* [ATLAS Collaboration], *JHEP* **1501**, 069 (2015) [arXiv:1409.6212 [hep-ex]].
- [22] G. Aad *et al.* [ATLAS Collaboration], *JHEP* **1504**, 117 (2015) [arXiv:1501.04943 [hep-ex]].
- [23] V. Khachatryan *et al.* [CMS Collaboration], *Eur. Phys. J. C* **74**, no. 10, 3076 (2014) [arXiv:1407.0558 [hep-ex]].
- [24] S. Chatrchyan *et al.* [CMS Collaboration], *Phys. Rev. D* **89**, no. 9, 092007 (2014) [arXiv:1312.5353 [hep-ex]].
- [25] S. Chatrchyan *et al.* [CMS Collaboration], *JHEP* **1401** (2014) 096 [arXiv:1312.1129 [hep-ex]].
- [26] V. Khachatryan *et al.* [CMS Collaboration], *Eur. Phys. J. C* **75**, no. 6, 251 (2015) [arXiv:1502.02485 [hep-ex]].
- [27] S. Chatrchyan *et al.* [CMS Collaboration], *Phys. Rev. D* **89**, no. 1, 012003 (2014) [arXiv:1310.3687 [hep-ex]].
- [28] S. Chatrchyan *et al.* [CMS Collaboration], *JHEP* **1405**, 104 (2014) [arXiv:1401.5041 [hep-ex]].
- [29] The W and Z bosons share a common reduced coupling here due to the custodial symmetry in the 2HDM. If custodial symmetry gets broken in some other models, one has to distinguish the WBF and ZBF couplings in the VBF processes and also the WH and ZH couplings.
- [30] A. Djouadi, *Phys. Rept.* **457**, 1 (2008) [hep-ph/0503172].
- [31] A. Djouadi, *Phys. Rept.* **459**, 1 (2008) [hep-ph/0503173].
- [32] G. C. Branco, P. M. Ferreira, L. Lavoura, M. N. Rebelo, M. Sher and J. P. Silva, *Phys. Rept.* **516**, 1 (2012) [arXiv:1106.0034 [hep-ph]].

- [33] A. Denner, S. Heinemeyer, I. Puljak, D. Rebuszi and M. Spira, Eur. Phys. J. C **71**, 1753 (2011) [arXiv:1107.5909 [hep-ph]].
- [34] <https://twiki.cern.ch/twiki/bin/view/LHCPhysics/CERNYellowReportPageAt7TeV>
- [35] <https://twiki.cern.ch/twiki/bin/view/LHCPhysics/CERNYellowReportPageAt8TeV>
- [36] F. Caola and K. Melnikov, Phys. Rev. D **88**, 054024 (2013) [arXiv:1307.4935 [hep-ph]].
- [37] T. Han and Z. Liu, Phys. Rev. D **87**, no. 3, 033007 (2013) [arXiv:1210.7803 [hep-ph]].
- [38] J. E. Brau, R. M. Godbole, F. R. L. Diberder, M. A. Thomson, H. Weerts, G. Weiglein, J. D. Wells and H. Yamamoto, arXiv:1210.0202 [hep-ex].
- [39] http://cepc.ihep.ac.cn/preCDR/main_preCDR.pdf